IOPscience iopscience.iop.org

Home Search Collections Journals About Contact us My IOPscience

High-pressure effects on the Raman spectrum and the force constants of the rare-earth aluminium garnets ($RE_3Al_5O_{12}$)

This article has been downloaded from IOPscience. Please scroll down to see the full text article.

2002 J. Phys.: Condens. Matter 14 3875

(http://iopscience.iop.org/0953-8984/14/15/303)

View the table of contents for this issue, or go to the journal homepage for more

Download details:
IP Address: 171.66.16.104
The article was downloaded on 18/05/2010 at 06:27

Please note that terms and conditions apply.

INSTITUTE OF PHYSICS PUBLISHING JOURNAL OF PHYSICS: CONDENSED MATTER

J. Phys.: Condens. Matter **14** (2002) 3875–3890 PII: S0953-8984(02)34659-9

High-pressure effects on the Raman spectrum and the force constants of the rare-earth aluminium garnets ($RE_3Al_5O_{12}$)

K Papagelis[1], J Arvanitidis[1], G Kanellis[1], S Ves[1,3] and G A Kouroukli[2]

[1] Physics Department, Aristotle University of Thessaloniki, GR-540 06 Thessaloniki, Greece
[2] Physics Division, School of Technology, Aristotle University of Thessaloniki, GR-540 06 Thessaloniki, Greece

E-mail: ves@auth.gr

Received 8 March 2002
Published 4 April 2002
Online at stacks.iop.org/JPhysCM/14/3875

Abstract

The pressure dependence of the Raman-active modes of the rare-earth aluminium garnet compounds ($RE_3Al_5O_{12}$, RE: Tb, Dy, Tm, Yb, Lu) has been measured at room temperature and discussed in terms of the rigid-ion model (RIM). The Raman modes in the high-frequency region ($\omega > 650\,cm^{-1}$) exhibit systematically larger pressure slopes (4–5.6 cm^{-1} GPa^{-1}) than the rest, which have slopes ranging between -0.1 and 3.3 cm^{-1} GPa^{-1}. The values of the Γ_i $(=\partial \ln \omega_i / \partial P)$ parameters show that the corresponding bonding in the $RE_3Al_5O_{12}$ family is nearly of the same nature and order of magnitude. No pressure-induced phase transitions could be detected up to 25 GPa. Using the RIM, the pressure dependence (up to 10 GPa) of the first-neighbour stretching and bending force constants for the Al–O (in the octahedra and tetrahedra) and RE–O bonds (in the dodecahedra) of the $Yb_3Al_5O_{12}$, $Dy_3Al_5O_{12}$ and $Tm_3Al_5O_{12}$ has been calculated. The calculated force constants show that the corresponding bonds in the samples investigated are of comparable strength and their pressure variation is quite similar. Furthermore, it has been found that they increase according to the sequence dodecahedra → octahedra → tetrahedra and that the compressibility follows the same trend, while the electronic configuration of the dodecahedral cation might play a role in the total compressibility.

1. Introduction

Garnets are mainly oxides, which crystallize in the body-centred cubic (bcc) lattice with space group symmetry $Ia3d$ (O_h^{10}) [1]. They contain four molecular units with chemical form $\{C_3\}[A_2](D_3)O_{12}$ in their primitive cell. In the case of the rare-earth garnets, C can be any

[3] Author to whom any correspondence should be addressed.

 © 2002 IOP Publishing Ltd Printed in the UK

one of the 14 well-known rare-earth ions or yttrium, while A and D can be any of Al^{3+}, Ga^{3+} or Fe^{3+} or other suitable atom combinations. The $Gd_3Sc_2Ga_3O_{12}$ garnet lattice is a particularly efficient host crystal for light-emitting ions such as Er^{+3} or Nd^{+3}, having emission characteristics for laser application in the visible region around 550 nm, in the NIR between 850 and 1700 nm and between 2.7 and 3 μm [2]. Devices based on garnet compounds, as laser-active media, are extremely attractive for many applications such as medical surgery, optical communications and coherent laser radar. Some doped oxide garnet materials have found applications as optical pressure sensors [3, 4], while garnets having an ordered or mixed structure have attracted attention because of their potential as starting materials in microelectronics and acoustoelectronics [5]. Despite the fact that aluminium garnet phases were believed to be absent in the Earth's lower mantle [6], due to phase transitions of garnets to silicate perovskites at high pressure, recent observations of a new tetragonal almandine–pyrope phase ($Mg_3Al_2Si_3O_{12}$) as inclusions in lower-mantle diamonds [7] have revived the interest in the role that garnets may play in the stability of the Earth's lower mantle.

The complexity of the crystal structure of the $RE_3Al_5O_{12}$ compounds (80 atoms per primitive cell) gives rise to a very rich Raman and infrared (IR) spectrum with well-defined features. In fact, group theory predicts 25 Raman-active modes ($3A_{1g}+8E_g+14T_{2g}$) and 17 IR-active modes ($17T_{1u}$). The IR and Raman spectra for the majority of the garnet family members under normal conditions have already been studied, a long time ago [8–12]. However, some of the Raman modes predicted by group theory were not observed experimentally, while the symmetry assignment of certain Raman-active modes, mainly the T_{2g} modes, is still debated in the literature [6,7,10,11]. The vibrational behaviour and the electronic structure of the rare-earth aluminium garnets have not been studied theoretically, up to now, except for in a few recent studies, namely, a lattice dynamical analysis based on the rigid-ion model (RIM) [13], band-structure calculations for $Y_3Al_5O_{12}$ based on first-principles local density theory [14] and, finally, calculations of the phonon density of states for aluminosilicate garnets based on the shell model using semi-empirical interatomic potentials [15]. It is well known that the optical properties of an ion, used as the active medium and located in a lattice site, strongly depend on the electron–phonon interaction in the host crystal. In this framework, knowledge of the vibrational properties of the host crystal is necessary in order to understand all aspects of the optical spectroscopy in these materials. The structural stability of the $RE_3Al_5O_{12}$ compounds, under external perturbations (like pressure or temperature), is also of great importance. Moreover, the application of high pressure simulates the lattice deformation caused by the replacement of a rare-earth ion by another with a different ionic radius and, therefore, the effects of pressure can be used to understand and estimate substitution effects in the optical properties of these materials. Therefore, such an investigation will contribute greatly to the understanding of the many critical features affecting the laser operation and may even become helpful in the discovery of new laser host materials.

In this work we present a detailed study of the Raman spectrum of $RE_3Al_5O_{12}$ (with RE being Tb, Dy, Tm, Yb or Lu) single crystals as a function of hydrostatic pressure up to 27 GPa. In addition, using the RIM, we have calculated the bond-bending (BB) and bond-stretching (BS) force constants as a function of volume. These experimental and theoretical findings are used to estimate the bond hierarchy as well as the pressure effect on the tetrahedral, octahedral and dodecahedral bonds in the $RE_3Al_5O_{12}$ compounds.

2. Experimental details

The $RE_3Al_5O_{12}$ samples were prepared by VanUitert and they have been made available to us by Dr A Jayaraman (AT&T Bell Laboratories, USA). Unpolarized Raman spectra of

unoriented $RE_3Al_5O_{12}$ samples were recorded by using two different experimental set-ups. The first set-up consisted of a SPEX 1401 double monochromator (1800 g mm^{-1}) utilizing a Peltier-cooled PM tube with GaAs photocathode, having a spectral width of $\sim$2.5 cm^{-1}. The spectra were recorded in the back-scattering geometry. The second set-up consisted of a triple monochromator (DILOR XY-500) equipped with a CCD (EG&G 1433-C) liquid-nitrogen-cooled detector system having a spectral width of $\sim$4 cm^{-1}. The spectra were recorded in the back-scattering geometry using an OLYMPUS microscope system for image processing. The 514.5 nm line of an Ar^+ laser was used for excitation and the laser power, measured directly before using the diamond anvil cell, was 25 mW. High pressure was generated using a diamond anvil cell of Mao and Bell type [16]; methanol–ethanol 4:1 mixture was used as the pressure-transmitting medium, which ensures good hydrostatic conditions up to $\sim$11 GPa with a divergence smaller than 2.5% for pressures up to 20 GPa [17] due to the solidification of the pressure-transmitting medium. Nevertheless, these non-hydrostatic components are the main reason for a noticeable broadening of the recorded Raman peaks in this pressure range. The well-known ruby fluorescence technique was used for pressure calibration [18].

3. Experimental results

The Raman spectra at room temperature and various pressures of $Tb_3Al_5O_{12}$ in the frequency region 100–900 cm^{-1} are illustrated in figure 1(*a*). Under normal conditions the Raman spectrum of the material shows 12 well-resolved phonon peaks (vertical lines in figure 1(*a*)) instead of the 25 Raman-active modes predicted by theory. The main reason for this is certain accidental degeneracies and/or relatively low Raman scattering efficiencies for some of the phonons. A considerable broadening of the Raman peaks, observed at higher pressure, may be caused by several factors, with the non-hydrostatic nature being the predominant one and the degeneracy in several phonon frequencies also contributing. The observed frequencies at ambient pressure agree well with those reported earlier in the literature [10]. The differences do not exceed 3 cm^{-1} except for the peaks at 326 cm^{-1} (E_g) and 774 cm^{-1} (A_{1g}) which were observed by Mace *et al* [10] at 339 and 787 cm^{-1}, respectively. The pressure dependence of the observed Raman frequencies is plotted in figure 1(*b*). The open (solid) symbols denote data taken with increasing (decreasing) pressure. The phonon frequencies were obtained by fitting Lorentzian lineshapes to the experimental data after background subtraction. In table 1 all the observed phonon frequencies and the corresponding pressure coefficients are tabulated along with their symmetry assignments. From figure 1(*b*) we see that all modes exhibit a linear pressure blue-shift over the whole pressure region investigated, and only the phonon mode at 850 cm^{-1} exhibits an almost superlinear pressure response. At ambient pressure the peak at $\sim$370 cm^{-1} consists of two normal modes of symmetry species A_{1g} and T_{2g}, which are accidentally degenerate, as can be deduced from figure 1(*a*). The application of pressure results in the clear separation of the two components, as it is evident from figure 1(*b*). This is due to the difference in their pressure response (see table 1) and not to symmetry breaking.

The Raman spectra at room temperature and various pressures of $Dy_3Al_5O_{12}$ are illustrated in figure 2(*a*), while the pressure dependence of the observed Raman frequencies is shown in figure 2(*b*). Under normal conditions, 16 Raman peaks have been observed and their frequencies agree well with those reported in the literature [9, 10]. We mention that in the measurements of Wadsack *et al* [9], the Raman peak at 110 cm^{-1} has not been observed, while the peaks at 746 cm^{-1} (E_g), 775 cm^{-1} (A_{1g}) and 846 cm^{-1} (T_{2g}), observed in the present work, have been recorded at 757, 790 and 854 cm^{-1} by Mace *et al* [10] and at 753, 781 and 849 cm^{-1} by Wadsack *et al* [9], respectively. With increasing pressure the Raman peaks shift to higher frequencies (figure 2(*b*), table 1) without significant changes in their lineshapes or relative

Table 1. Experimental and theoretically calculated phonon frequencies and pressure coefficients, as well as the Γ_i $(=\partial \ln \omega_i / \partial P)$ parameters for the compounds $Tb_3Al_5O_{12}$, $Dy_3Al_5O_{12}$, $Tm_3Al_5O_{12}$, $Yb_3Al_5O_{12}$ and $Lu_3Al_5O_{12}$.

	$Tb_3Al_5O_{12}$			$Dy_3Al_5O_{12}$					$Tm_3Al_5O_{12}$				
	Experiment			Experiment			Theory		Experiment			Theory	
Symmetry	ω_i (cm^{-1})	$\partial\omega_i/\partial P$ (cm^{-1} GPa^{-1})	Γ_i (GPa^{-1})	ω_i (cm^{-1})	$\partial\omega_i/\partial P$ (cm^{-1} GPa^{-1})	Γ_i (GPa^{-1})	ω_i (cm^{-1})	$\partial\omega_i/\partial P$ (cm^{-1} GPa^{-1})	ω_i (cm^{-1})	$\partial\omega_i/\partial P$ (cm^{-1} GPa^{-1})	Γ_i (GPa^{-1})	ω_i (cm^{-1})	$\partial\omega_i/\partial P$ (cm^{-1} GPa^{-1})
T_{2g}	—	—	—	110[a]	1.3	11.8	122	0.9	107[a]	1.0	9.3	120	0.8
E_g	—	—	—	129[a]	0.5	3.9	125	0.3	127[a]	0.7	5.5	124	0.5
T_{2g}	—	—	—	166[a]	1.2	7.2	190	1.3	157[a]	1.9	12.0	170	1.5
T_{2g}	238	2.2	9.2	239[a]	2.2	9.2	233	2.2	235[a]	2.5	10.6	233	2.0
T_{2g}	263	1.3	4.9	260[a]	1.7	6.5	247	1.9	259[a]	1.8	6.9	244	1.8
T_{2g}	293	2.2	7.5	292	2.4	8.2	305	2.8	295[a]	2.4	8.1	296	2.6
E_g	—	—	—	—	—	—	296	2.9	—	—	—	290	2.4
E_g	326	1.9	5.8	323[a]	2.4	7.4	325	2.6	324[a]	2.7	8.3	315	2.7
T_{2g}	—	—	—	—	—	—	336	3.0	—	—	—	333	2.6
A_{1g}	369	1.6	4.3	367	1.8	4.9	376	2.8	—	—	—	361	3.0
T_{2g}	374	3.2	8.6	371	3.4	9.2	377	3.1	367	3.5	9.5	370	3.2
E_g	395	2.4	6.1	396	2.4	6.1	378	2.9	389	2.5	6.4	364	2.4
T_{2g}	—	—	—	—	—	—	399	3.0	402	1.1	2.7	385	2.1
T_{2g}	—	—	—	—	—	—	492	3.6	—	—	—	478	3.3
E_g	—	—	—	—	—	—	505	4.0	—	—	—	490	3.5
E_g / T_{2g}	537	2.5	4.7	539	2.6	4.8	556 568	2.9 3.0	546	2.5	4.6	558 552	2.8 3.1
A_{1g}	558	2.3	4.1	557	2.6	4.7	555	3.1				543	3.0
T_{2g}	—	—	—	—	—	—	623	3.5	—	—	—	605	2.7
T_{2g}	686	4.9	7.1	686[a]	5.5	8.0	689	5.4	700[a]	5.6	8.0	700	5.4
E_g / T_{2g}	707	5.2	7.4	710	5.4	7.6	680 711	5.3 5.6	726	5.3	7.3	685 730	4.4 5.5
E_g	—	—	—	746[a]	5.4	7.2	750	5.4	765[a]	5.1	6.7	768	4.5
A_{1g}	774	4.2	5.4	775[a]	4.4	5.7	760	4.5	789[a]	4.2	5.3	760	4.1
T_{2g}	850	3.0[b]	3.5	846[a]	4.9	5.8	850	5.0	863	—	—	862	5.0

Table 1. (Continued)

	$Yb_3Al_5O_{12}$					$Lu_3Al_5O_{12}$		
	Experiment			Theory		Experiment		
Symmetry	ω_i (cm^{-1})	$\partial\omega_i/\partial P$ (cm^{-1} GPa^{-1})	Γ_i (GPa^{-1})	ω_i (cm^{-1})	$\partial\omega_i/\partial P$ (cm^{-1} GPa^{-1})	ω_i (cm^{-1})	$\partial\omega_i/\partial P$ (cm^{-1} GPa^{-1})	Γ_i (GPa^{-1})
T_{2g}	104[a]	1.3	12.5	116	1.0	107	−0.1	−0.9
E_g	126[a]	0.5	4.0	123	0.3	130	0.4	3.1
T_{2g}	158[a]	1.2	7.6	170	1.2	156	1.4	9.0
T_{2g}	235[a]	2.4	10.2	230	1.7	240	1.9	7.9
T_{2g}	258[a]	1.8	7.0	237	1.9	261	1.5	5.7
T_{2g}	—	—	—	300	2.2	—	—	—
E_g	303[a]	2.2	7.3	302	2.2	313	2.7	8.6
E_g	323[a]	2.6	8.6	321	2.7	330	2.2	6.7
T_{2g}	—	—	—	350	2.4	—	—	—
A_{1g}	—	—	—	361	2.9	375	1.5	4.0
T_{2g}	362	3.4	9.4	367	3.1	376	3.3	8.8
E_g	382	2.7	7.1	371	2.9	396	2.1	5.3
T_{2g}	—	—	—	397	3.0	415	1.9	4.6
T_{2g}	—	—	—	475	2.7	—	—	—
E_g	—	—	—	504	3.0	—	—	—
E_g	537[a]	2.2	4.1	539	2.5	537	2.0	3.7
T_{2g}	547[a]	2.5	4.6	560	2.6	551	2.2	4.0
A_{1g}	—	—	—	552	2.9			
T_{2g}	—	—	—	617	2.6	—	—	—
T_{2g}	707[a]	4.9	6.9	707	4.8	708	4.8	6.8
E_g	729	5.6	7.7	701	4.2	723	4.1	5.7
T_{2g}				737	5.0	736	4.5	6.1
E_g	772	4.3	5.6	773	4.5	773	4.4	5.7
A_{1g}	797	4.5	5.6	777	4.2	797	3.7	4.6
T_{2g}	867	—	—	870	4.5	869	—	—

[a] The marked frequencies are used as input in the fitting procedure.
[b] Parabolic fitting with $\partial\omega_i/\partial P = 3.0\ cm^{-1}\ GPa^{-1}$ and $\partial^2\omega_i/\partial^2 P = 0.1$.

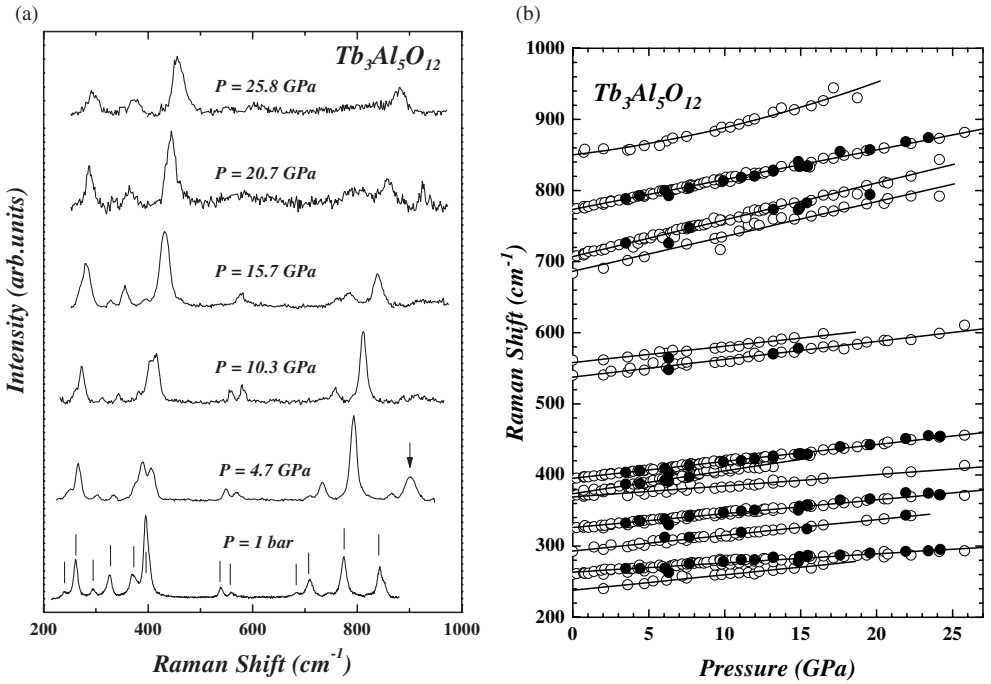

Figure 1. (*a*) Raman spectra of $Tb_3Al_5O_{12}$ at room temperature and various pressures. The vertical lines indicate the observed phonon peaks while the arrow indicates a methanol–ethanol peak. (*b*) The pressure dependence of the observed phonon modes of $Tb_3Al_5O_{12}$. The open (solid) symbols denote data taken with increasing (decreasing) pressure.

intensities. The peak at $\sim$370 cm^{-1} shows a pressure-induced splitting into two components in analogy to the case for $Tb_3Al_5O_{12}$.

The Raman spectra of $Tm_3Al_5O_{12}$ at various pressures and the pressure dependence of the observed phonon frequencies are displayed in figures 3(*a*) and (*b*), respectively. In the absence of any polarized Raman measurements, we have made the assignment of the observed Raman peaks in analogy to the assignment for the other members of the garnet family (table 1). Please note the apparent broadening of the Raman peaks for pressure above 3.4 GPa (figure 3(*a*)), due primarily to the weak Raman scattering efficiency of this particular compound along with the crossing tendency exhibited between several modes (see figure 3(*b*)), which makes clear resolution of nearby individual components difficult. The Raman spectra at various pressures and the pressure dependence of the phonon modes for $Yb_3Al_5O_{12}$ are presented in figures 4(*a*) and (*b*), respectively. The phonon frequencies for $Yb_3Al_5O_{12}$ are in good agreement with those reported earlier [10, 11]. For the above two compounds we have resolved only 15 out of 25 Raman-active modes and their pressure evolution can be followed up to 10 GPa, the highest pressure achieved in the present study. The pressure behaviour of the Raman modes of $Tm_3Al_5O_{12}$ and $Yb_3Al_5O_{12}$ is similar to that of the other $RE_3Al_5O_{12}$ compounds mentioned above. It is worth noticing that the peak at $\sim$370 cm^{-1} does not show the characteristic pressure-induced splitting, in two components, as is seen for $Tb_3Al_5O_{12}$ and $Dy_3Al_5O_{12}$—on the contrary, it shows a tendency to exhibit crossing for the case of $Tm_3Al_5O_{12}$.

Finally, in figure 5, the Raman spectra for various pressures (*a*) and the pressure dependence of the 18 observed Raman peaks (*b*) of $Lu_3Al_5O_{12}$ are illustrated. For this compound

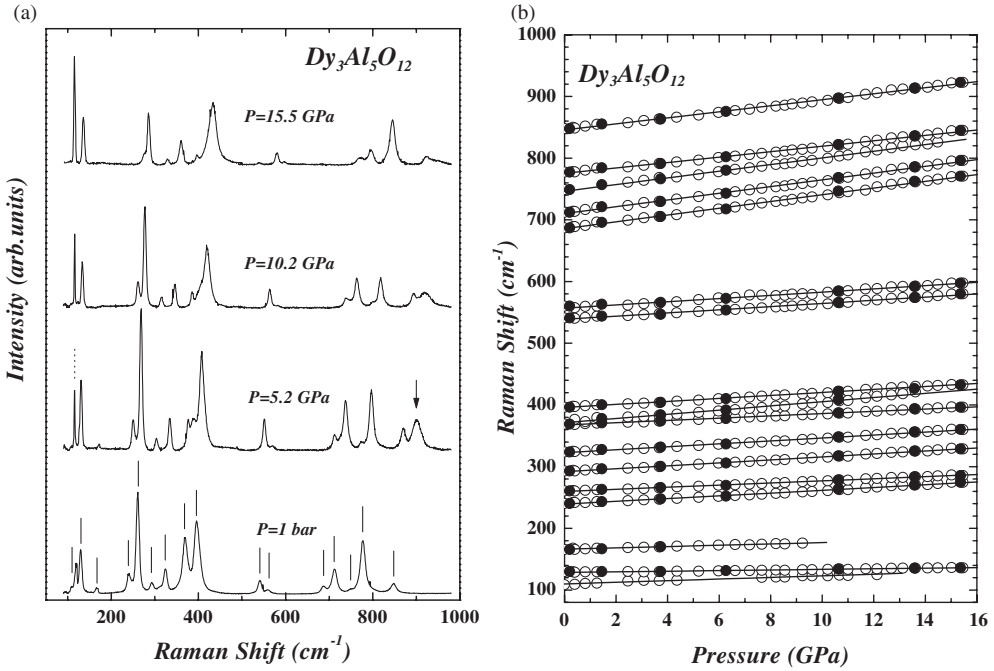

Figure 2. (*a*) Raman spectra of $Dy_3Al_5O_{12}$ at room temperature and various pressures. The vertical lines indicate the observed phonon peaks. The arrow and the dotted vertical line indicate a methanol–ethanol peak and an Ar^+ laser plasma line, respectively. (*b*) The pressure dependence of the observed phonon modes of $Dy_3Al_5O_{12}$. The open (solid) symbols denote data taken with increasing (decreasing) pressure.

also, the differences between the observed phonon frequencies and those reported earlier in the literature [11] do not exceed the spectral resolution of the experimental set-ups used. Note that the peaks at 340 and 351 cm^{-1} have not been recorded before. The origin of these lines is unknown and further investigation is needed, whereas the possibility that these peaks are due to spurious impurity-activated modes cannot be excluded. From figure 5(*b*) and table 1 it is evident that all observed frequencies exhibit a positive pressure shift, except for the mode at 108 cm^{-1}, which shows nearly zero or marginally negative slope. The peak at ∼370 cm^{-1} shows a pressure-induced splitting as in the case of $Tb_3Al_5O_{12}$ and $Dy_3Al_5O_{12}$. Similar behaviour is exhibited also by the peak at ∼730 cm^{-1}, which consists of two phonon modes with E_g and T_{2g} symmetry. Under normal conditions, the higher-frequency line of T_{2g} symmetry is very intense and dominates the Raman spectrum in the frequency region around 730 cm^{-1}. At higher pressure the difference in intensity of the two components is not as pronounced. However, their pressure evolution could be followed easily up to the highest pressure achieved, because their pressure responses are slightly different, thus making their separation easier.

Overall, the Raman spectra of the materials investigated (figures 1–5) are very similar and their study is facilitated by separating them into three frequency regions:

(i) the high-frequency region (650–900 cm^{-1});
(ii) the intermediate-frequency region (500–600 cm^{-1}); and
(iii) the low-frequency region ($\omega < 500$ cm^{-1}).

This classification allows us to interpret some of the observed Raman modes in terms of the isolated AlO_4 molecular subunit vibrations in the structure of the $RE_3Al_5O_{12}$ compounds [19].

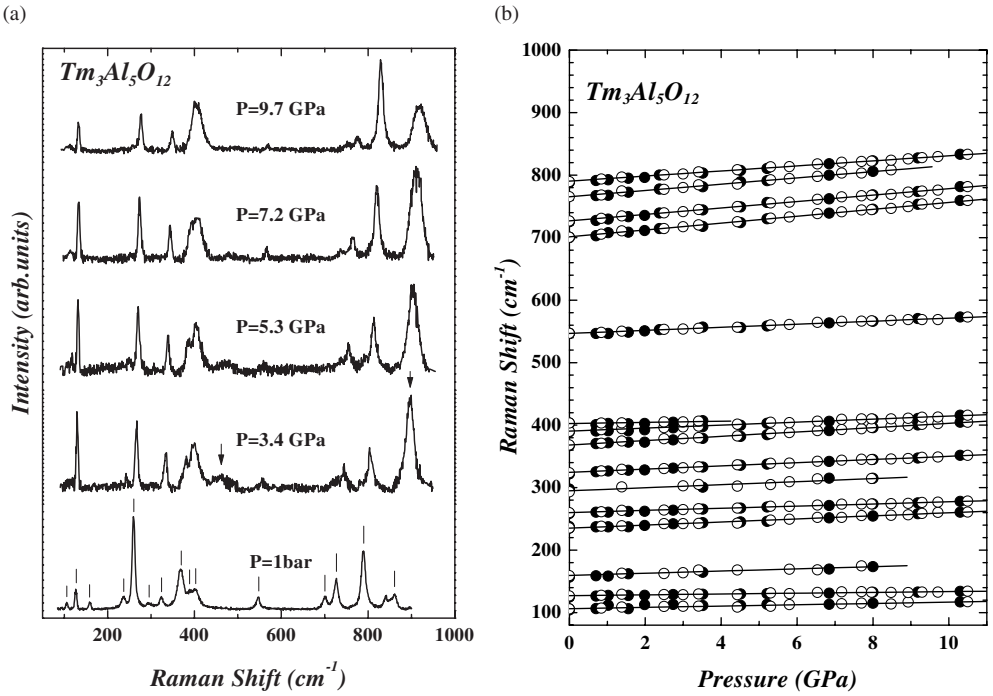

Figure 3. (*a*) Raman spectra of $Tm_3Al_5O_{12}$ at room temperature and various pressures. The vertical lines indicate the observed phonon peaks, while the arrow represents a methanol–ethanol peak. (*b*) The pressure dependence of the observed phonon modes of $Tm_3Al_5O_{12}$. The open (solid) symbols denote data taken with increasing (decreasing) pressure.

The corresponding pressure slopes for all $RE_3Al_5O_{12}$ materials investigated have quite similar values, as can be seen from table 1. This reveals the fact that the pressure evolution of the Raman mode frequencies is almost insensitive to the specific mass and the different electronic configurations of the various rare-earth ions present in the specific garnet. This might be understood by considering the fact that all modes involve motions of more than one type of atomic species, washing out the small mass differences. On the other hand, the modes in the high-frequency region ($\omega > 650$ cm^{-1}) exhibit systematically larger pressure coefficient values (4–5.6 cm^{-1} GPa^{-1}) than the rest. Therefore, these modes should be affected more by the application of the pressure, as they involve significant stretching components of the tetrahedral and octahedral bonds [13]. The pressure slopes of the low-frequency-region modes range between -0.1 and 2.7 cm^{-1} GPa^{-1} except for the mode at $\sim$370 cm^{-1} which shifts at a rate of $\sim$3.3 cm^{-1} GPa^{-1}. These modes are less sensitive to the pressure increase because they are related to the angular displacements or forces having small BS components of the basic polyhedra in the garnet compounds [13].

From the pressure evolution of the phonon frequencies, there is no evidence of pressure-induced phase transitions in the pressure region investigated. Hua *et al* [20], using a synchrotron x-ray diffraction technique, reported that polycrystalline gadolinium scandium gallium garnet ($Gd_3Sc_2Ga_3O_{12}$) undergoes a pressure-induced amorphization at 58 $\pm$ 3 GPa and ambient temperature, while $Y_3Al_5O_{12}$ retains its crystalline cubic phase up to 101 $\pm$ 4 GPa [21], making these materials extremely stable under pressure application.

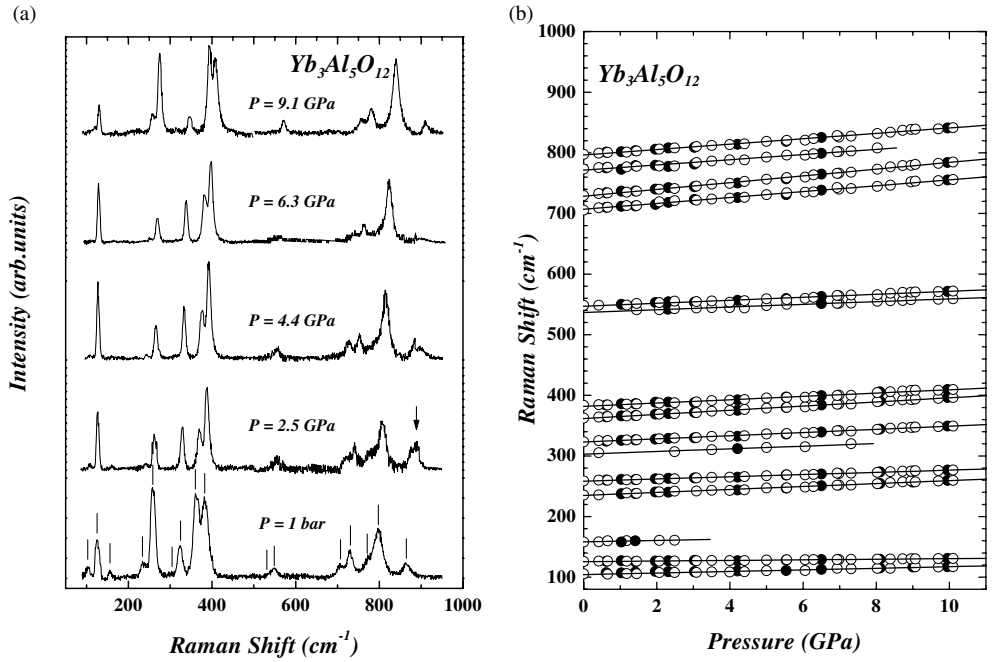

Figure 4. (*a*) Raman spectra of $Yb_3Al_5O_{12}$ at room temperature and for various pressures. The vertical lines indicate the observed phonon peaks, while the arrow represents a methanol–ethanol peak. (*b*) The pressure dependence of the observed phonon modes of the $Yb_3Al_5O_{12}$. The open (solid) symbols denote data taken with increasing (decreasing) pressure.

4. Calculation of the force constants and their pressure dependence

As already mentioned in the introduction, the crystal structure of the $RE_3Al_5O_{12}$ compounds is very complex. It contains 80 atoms in the primitive cell distributed in the following way:

(i) twelve RE ions occupy dodecahedral sites;
(ii) eight Al ions are located in octahedral sites;
(iii) twelve Al ions occupy tetrahedral sites; and
(iv) the oxygens are located in 48 general positions.

Therefore, the garnet crystal structure consists of some basic polyhedra (tetrahedra, octahedra and dodecahedra), each having a proper cation at their centre, surrounded by the proper number of oxygen ions (OX). Each oxygen belongs to two dodecahedra, one tetrahedron and one octahedron. The Al–O distance in the tetrahedra is the shortest cation–anion distance ($\sim$1.77 Å), while the same distance in the octahedra is $\sim$10% larger. The RE–O distance in the dodecahedra is 33% larger than the shortest one.

In order to elucidate the mode assignment of the observed Raman frequencies, we have performed lattice dynamical calculations, using a RIM, for the $RE_3Al_5O_{12}$ gernets in an earlier work [13]. In this model, the short-range interactions between two atoms κ and κ', up to the fourth neighbour, are described by the Born–Mayer potential $V^{SR}_{\kappa\kappa'}(r) = V_0 \exp(-r/[\sigma_\kappa + \sigma_{\kappa'})]$ where the σ_κ, $\sigma_{\kappa'}$ and V_0 are the Born–Mayer parameters, respectively. The parameters $\sigma_\kappa + \sigma_{\kappa'}$ and V_0 describe the range and the strength of the repulsive interactions. The long-range electrostatic contribution is a slowly convergent series and the Ewald method has been used for its calculation [22]. The interactions in the $RE_3Al_5O_{12}$ crystals have been described by a

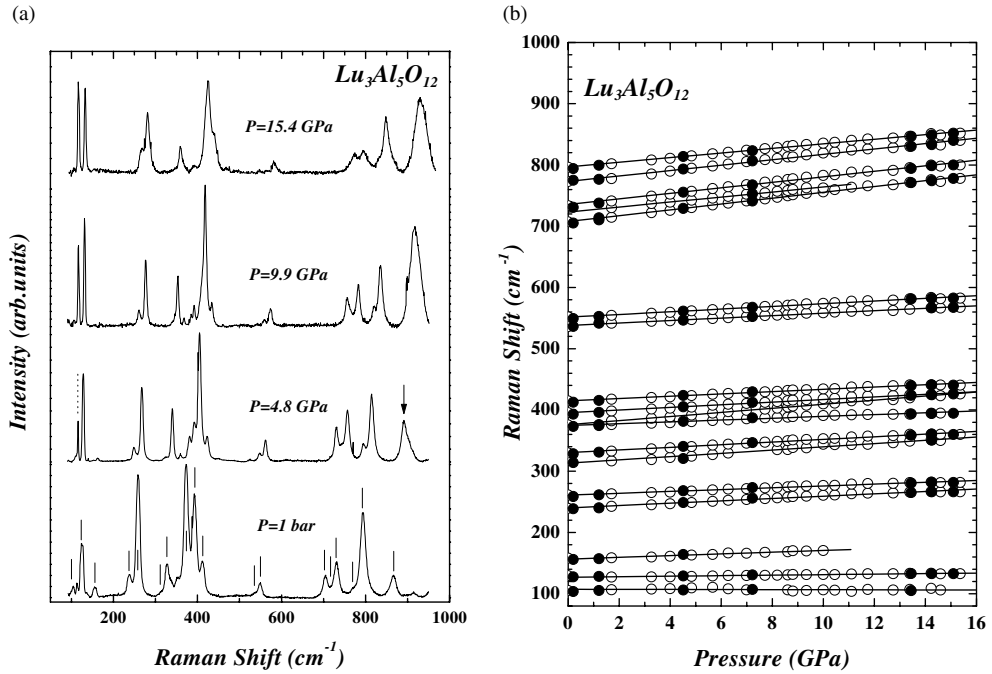

Figure 5. (*a*) Raman spectra of $Lu_3Al_5O_{12}$ for various pressures at room temperature. The vertical solid lines indicate the observed phonon peaks. The arrow and the dotted vertical line indicate a methanol–ethanol peak and an Ar^+ laser plasma line, respectively. (*b*) The pressure dependence of the observed phonon modes of $Lu_3Al_5O_{12}$. The open (solid) symbols denote data taken with increasing (decreasing) pressure.

set of nine parameters σ_{ALT}, Z_{ALT}, σ_{ALO}, Z_{ALO}, σ_{RE}, Z_{RE}, σ_{OX}, Z_{OX} and V_0, where their indices refer to the tetrahedral Al ion (ALT) and octahedral Al ion (ALO), to the rare-earth (RE) ions and to the OX. Additionally, the Z_i (i: ALT, ALO, RE, OX) parameters represent the effective charges of the corresponding ions. The choice of the above model, although not unique, is in fact imposed by the lack of adequate reliable experimental data, in order to minimize the number of independent parameters to be fitted. We have performed the lattice dynamical calculations for the $Dy_3Al_5O_{12}$, $Tm_3Al_5O_{12}$ and $Yb_3Al_5O_{12}$ compounds for which the most complete set of Raman and IR measurements are available. The values of the parameters have been determined by least-squares fitting of the theoretical values to the unambiguously assigned experimental Raman and IR frequencies. The use of IR frequencies as input data for the fitting procedure is necessary for obtaining a reliable set of values for the fitted parameters. This is, in particular, true for the estimation of the ionic effective charges, since the subspace of just the Raman modes is not adequate. The Raman frequencies used in our fitting procedure are marked with a superscript 'a' in table 1. The corresponding IR frequency values are taken from [8, 12]. Altogether, the frequencies used for the determination of the parameters number around 25, depending on the available experimental data. As regards the ionic effective charges of the $RE_3Al_5O_{12}$ structure, the parameter values (see table 2) indicate that: (i) the RE ions have larger effective charges (Z_{RE}) than the other cations in all three compounds; and (ii) the octahedral Al ions have larger effective charges (Z_{ALO}) than the tetrahedral Al ions (Z_{ALT}) except for those of the $Dy_3Al_5O_{12}$ structure which exhibit the opposite behaviour.

Table 2. The effective charges and the BS (L) and BB (T) force constants calculated using the RIM for $Dy_3Al_5O_{12}$, $Tm_3Al_5O_{12}$ and $Yb_3Al_5O_{12}$. The force constants and the effective charges were determined by fitting to the Raman and IR experimental data.

	$Dy_3Al_5O_{12}$	$Tm_3Al_5O_{12}$	$Yb_3Al_5O_{12}$
Z_{ALO} (e)	1.519	1.962	1.890
Z_{RE} (e)	2.470	2.127	2.234
Z_{ALT} (e)	1.658	1.616	1.617
Z_{OX} (e)	−1.285	−1.263	−1.278
L_{tetr} (N m^{-1})	401.18	409.70	415.40
T_{tetr} (N m^{-1})	40.05	40.87	41.41
L_{oct} (N m^{-1})	181.21	200.98	199.21
T_{oct} (N m^{-1})	16.82	18.82	18.59
L_{dod} (N m^{-1})	207.70	188.89	196.77
T_{dod} (N m^{-1})	20.40	18.28	19.09

From the short-range parameter values, we have calculated the Bond Stretching (BS) ($L = \mathrm{d}^2V_{\kappa\kappa'}(r)/\mathrm{d}^2r$) and the Bond Bending (BB) ($L = (1/r)\,\mathrm{d}V_{\kappa\kappa'}(r)/\mathrm{d}r$) force constants for the first-neighbour cation–oxygen bonds (table 2). The short-range force constants for the tetrahedral Al–O bonds (L_{tetr}, T_{tetr}) are almost double those of the Al–O bonds in the octahedra (L_{oct}, T_{oct}) and the RE–O bonds in the dodecahedra (L_{dod}, T_{dod}). The force constant values for the octahedra and dodecahedra are nearly the same. Our model calculations reveal that the tetrahedral Al–O bonds exhibit mostly a covalent character while the dodecahedral RE–O bonds an almost ionic character for all the materials investigated. Moreover, the eigenvectors [13] of the Raman-active modes located in the frequency region $\omega > 500$ cm^{-1} exhibit a higher degree of molecular character, which is related to the vibrations of the tetrahedral (AlO_4) and octahedral (AlO_6) molecular subunits. The rest of the modes are more complicated and correspond to a mixing of the molecular modes of the basic molecular subunits (tetrahedra, octahedra and dodecahedra).

The above-mentioned model calculations along with the observed similar frequency and pressure slope values of the Raman-active modes in the compounds under investigation clarify the symmetry assignment of the modes which are accidentally degenerate at normal conditions. Specifically, in the case of $Tb_3Al_5O_{12}$, $Dy_3Al_5O_{12}$ and $Lu_3Al_5O_{12}$ the component of the doubly degenerate peak at ∼370 cm^{-1}, having the lower pressure slope and the lower frequency, must be of A_{1g} symmetry while the second one must be of T_{2g} symmetry. As a consequence, the mode at ∼367 cm^{-1} (pressure slope 3.5 cm^{-1} GPa^{-1}) in $Tm_3Al_5O_{12}$ and the mode ∼362 cm^{-1} (pressure slope 3.4 cm^{-1} GPa^{-1}) of $Yb_3Al_5O_{12}$ must be of T_{2g} symmetry (table 1). It is important to note that the A_{1g} modes involve only motions of the OX while in the T_{2g} modes the cations are moving too. The much smaller pressure slope values of the T_{2g} mode can be related to the relative displacements of the cations instead of oxygens. Furthermore, the Raman peak at ∼390 cm^{-1} is also accidentally doubly degenerate and the two components have E_g and T_{2g} symmetry. For $Tm_3Al_5O_{12}$ and $Lu_3Al_5O_{12}$ these two components have been clearly recorded even under normal conditions as their accidental degeneracy is lifted. The mode having the lower frequency and the larger slope must be of E_g symmetry. Therefore, the mode at 395 cm^{-1} (2.4 cm^{-1} GPa^{-1}) of $Tb_3Al_5O_{12}$, the mode at 396 cm^{-1} (2.4 cm^{-1} GPa^{-1}) of $Dy_3Al_5O_{12}$ and the mode at 382 cm^{-1} (2.7 cm^{-1} GPa^{-1}) of $Yb_3Al_5O_{12}$ must be assigned to the E_g symmetry. The above arguments explain the crossing behaviour in the pressure dependence of the Raman frequencies, observed for $Tb_3Al_5O_{12}$, $Dy_3Al_5O_{12}$ and $Lu_3Al_5O_{12}$ compounds, of the T_{2g} and E_g modes at ∼370 and ∼390 cm^{-1}.

The three Raman modes in the frequency region $\omega < 200\,\mathrm{cm}^{-1}$ exhibit the smallest slopes. The mode at $110\,\mathrm{cm}^{-1}$ corresponds to the translational relative motion of an atomic unit which consists of one tetrahedral Al (with the oxygens belonging to it) and one of the two RE ions which are close to the tetrahedral Al ions [13]. This mode in $Lu_3Al_5O_{12}$ shows a very small negative slope ($-0.1\ \mathrm{cm}^{-1}\ \mathrm{GPa}^{-1}$). The reason for that is possibly related to the existence of 5d electrons in $Lu_3Al_5O_{12}$, but further investigation is needed in order to clarify the reason for this negative slope. The other two modes cannot be directly associated with a translational motion of a particular molecular subunit.

In order to estimate the pressure effect on the bonds of the $RE_3Al_5O_{12}$ compounds we have performed calculations using the same RIM at different unit-cell volumes. In particular, we have calculated the pressure dependence of the short-range force constants by means of a uniform reduction of the crystal lattice, assuming that the harmonic approximation is valid for pressures up to 10 GPa. The volume dependence of the atomic positions for the $RE_3Al_5O_{12}$ compounds is calculated by using the Murnaghan equation [23]. We note that the bulk modulus (B_0) is not known for any member of the $RE_3Al_5O_{12}$ family. Therefore, we have considered the value of 200 GPa for B_0, for all materials, which is compatible with the experimental value for $Y_3Al_5O_{12}$ [24] and $RE_3Fe_5O_{12}$ [5] and the relatively high hardness of the garnet compounds. Additionally, we have chosen, for the first pressure derivative of the bulk modulus ($\partial B/\partial P$) the typical value of 4 [25]. The lack of high-pressure IR experimental data introduces a restriction on the set of adjustable parameters to be used for the theoretical calculation of the pressure dependence of the force constants: the adjustable parameters, used in the pressure dependence calculations, had to be determined only from the measured high-pressure Raman data, which are insufficient for making an unambiguous unique determination of the fitting parameters. In order to overcome this ambiguity, the effective charges of the cations and the oxygens as well as the strength parameter V_0 have been treated as volume independent. This approximation is quite reasonable, as it is well known that for a relative volume change of 3% the effective charges, at least in semiconductors, remain almost constant [26]. Therefore, we have assumed intuitively that the pressure variation causes only a change in the σ_i-parameters, which is expected to be the parameter most sensitive to the volume reduction. Obviously, this assumption will lead to an overestimation of the pressure dependence of the force constants, but the goal here is to compare their relative and not their absolute values as well as to look for trends in the family of compounds investigated.

The calculated frequencies for all Raman-active modes at normal pressure along with their pressure coefficients for $Dy_3Al_5O_{12}$, $Tm_3Al_5O_{12}$ and $Yb_3Al_5O_{12}$ are summarized in table 1. The choice of the particular compounds on which to perform our theoretical calculation was based solely on the completeness of the available experimental data and on the fact that the results obtained should be, more or less, representative for all the aluminium garnets. The agreement between calculated and experimental Raman frequencies values is quite satisfactory. In particular, the model predicts very well the degenerate frequency values at $\sim 370\ \mathrm{cm}^{-1}$ of the A_g and T_g modes. It is very interesting to note the very good agreement of the calculated and the corresponding experimentally determined pressure coefficients, which supports the validity of our assumption about the negligible volume dependence of effective charges.

The pressure dependence, up to 10 GPa, of the first-neighbour BS (L) and BB (T) force constants for the Al–O bonds of the tetrahedra (L_{tetr}, T_{tetr}) and octahedra (L_{oct}, T_{oct}) and the RE–O bonds of the dodecahedra (L_{dod}, T_{dod}) for $Dy_3Al_5O_{12}$ and $Yb_3Al_5O_{12}$ are presented in figure 6. The pressure behaviour of the force constants for $Tm_3Al_5O_{12}$ is similar to that of the force constants for $Yb_3Al_5O_{12}$. In table 3 the first-neighbour BS and BB force constants and their pressure coefficients for $Dy_3Al_5O_{12}$, $Tm_3Al_5O_{12}$ and $Yb_3Al_5O_{12}$ are tabulated. From figure 6 it is evident that the force constants show a linear dependence upon pressure (volume).

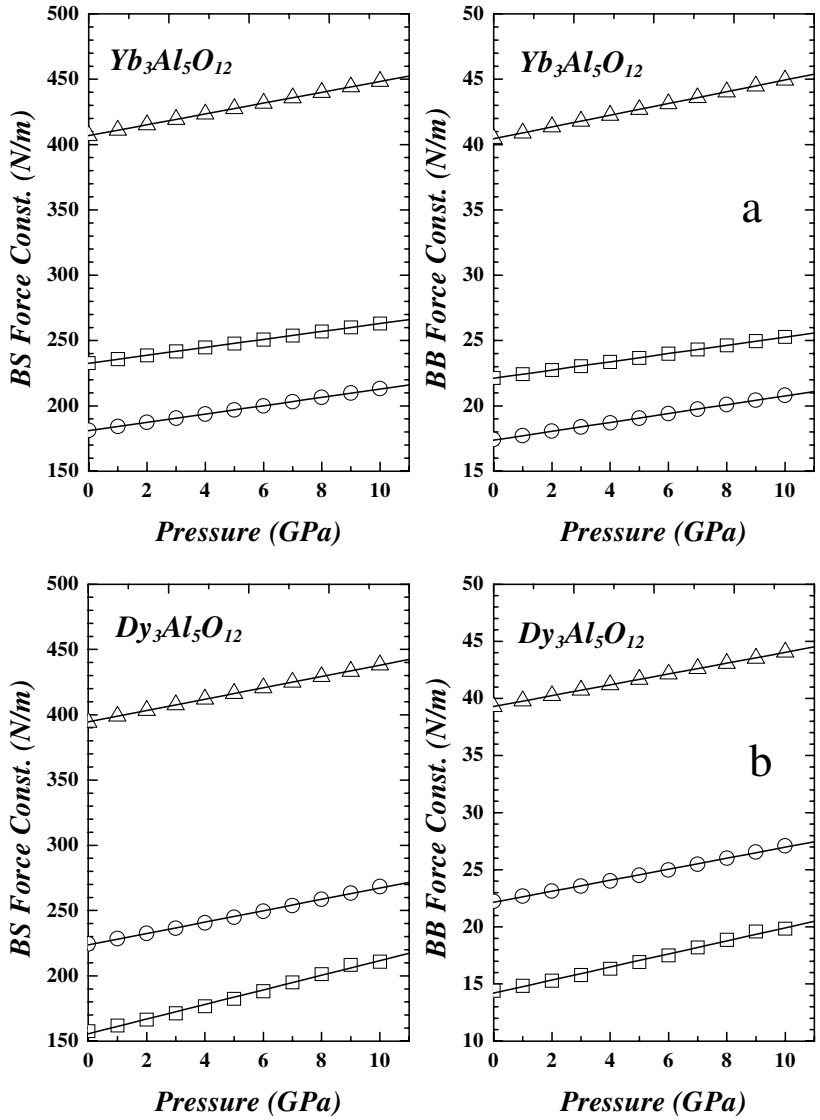

Figure 6. The pressure dependence of the BS and BB force constants of the tetrahedral (triangles) and octahedral (squares) Al–O bonds and the dodecahedral (circles) RE–O bonds for $Yb_3Al_5O_{12}$ (*a*) and $Dy_3Al_5O_{12}$ (*b*). The top x-axis gives, in all graphs, the relative volume change ($\Delta V/V_0$).

Moreover, from table 3 we infer that for $Tm_3Al_5O_{12}$ and $Yb_3Al_5O_{12}$ compounds the pressure slope of the Al_{tetr}–O BS force constant ($\partial L_{tetr}/\partial P$) is larger than the corresponding ones for the Al_{oct}–O and RE–O bonds, while the $\partial L_{dod}/\partial P$ slope of the RE–O bond is larger than that for the Al_{oct}–O bonds. In contrast, in $Dy_3Al_5O_{12}$ the pressure slope of the Al_{oct}–O BS force constant is larger than those of the corresponding ones for the Al_{tetr}–O and RE–O bonds. Finally, we point out that the BB force constants exhibit the same trends as the BS ones for the three materials investigated theoretically.

The trend in the calculated force constants indicates that for the Tm (Yb) aluminium garnets the 'compressibility' and 'distortion' of the various molecular units increases according

Table 3. The BS (L) and the BB (T) force constants, their pressure coefficients and the pressure parameters Γ_k ($=(1/2k)\partial k/\partial P$) for $Dy_3Al_5O_{12}$, $Tm_3Al_5O_{12}$ and $Yb_3Al_5O_{12}$. Note that the force constants were determined by fitting to the measured high-pressure Raman data.

	$Dy_3Al_5O_{12}$	$Tm_3Al_5O_{12}$	$Yb_3Al_5O_{12}$
L_{tetr} (N m^{-1})	394.53	403.55	406.90
$\partial L_{\text{tetr}}/\partial P$ (N m^{-1} GPa^{-1})	4.35	4.66	4.14
$\Gamma_{L_{\text{tetr}}}$ (10^{-3} GPa^{-1})	5.51	5.77	5.09
T_{tetr} (N m^{-1})	39.30	40.18	40.45
$\partial T_{\text{tetr}}/\partial P$ (N m^{-1} GPa^{-1})	0.47	0.52	0.45
$\Gamma_{T_{\text{tetr}}}$ (10^{-3} GPa^{-1})	5.98	6.47	5.56
L_{oct} (N m^{-1})	155.71	200.69	232.65
$\partial L_{\text{oct}}/\partial P$ (N m^{-1} GPa^{-1})	5.59	2.29	3.03
$\Gamma_{L_{\text{oct}}}$ (10^{-3} GPa^{-1})	17.95	5.70	6.51
T_{oct} (N m^{-1})	14.20	18.79	22.10
$\partial T_{\text{oct}}/\partial P$ (N m^{-1} GPa^{-1})	0.57	0.23	0.32
$\Gamma_{T_{\text{oct}}}$ ($\times 10^{-3}$ GPa^{-1})	20.07	6.12	7.24
L_{dod} (N m^{-1})	223.67	183.83	180.94
$\partial L_{\text{dod}}/\partial P$ (N m^{-1} GPa^{-1})	4.37	3.55	3.19
$\Gamma_{L_{\text{dod}}}$ ($\times 10^{-3}$ GPa^{-1})	9.77	9.66	8.82
T_{dod} (N m^{-1})	22.16	17.73	17.37
$\partial T_{\text{dod}}/\partial P$ (N m^{-1} GPa^{-1})	0.48	0.38	0.34
$\Gamma_{T_{\text{dod}}}$ (10^{-3} GPa^{-1})	10.83	10.72	9.79

to the sequence dodecahedra → octahedra → tetrahedra, assuming that they are manifested by the stretching and bending force constants, respectively. In contrast, for $Dy_3Al_5O_{12}$ it seems that the order reverts for dodecahedra and octahedra. Our finding is in line with the conclusion of Hazen *et al* [27] who stated that octahedral and tetrahedral networks in garnets control the compressibility, with the eightfold-coordinated cation in the dodecahedron playing a primary role. Later Zhang *et al* [28] claimed that the compression in aluminosilicate garnets ($M_3Al_2SiO_4$, with M = Mg, Fe, Mn, Ca) could be governed also by the degree of kinking of the angle M–O–Si and the electronic configuration of the dodecahedral cations. The higher the valence state of the dodecahedral cation, the lower the compressibility of the structure as a whole. The latter point might explain the observed reversal in $Dy_3Al_5O_{12}$, as in Dy the f shell is just half-filled.

The Grüneisen parameter, to a first approximation, is related to the volume-induced modifications of the force constants of the bonds participating in a normal mode. As the bulk modulus for the $RE_3Al_5O_{12}$ compounds under consideration here is not known and in order to compare the various forces in the garnet lattice, we use the parameters Γ_i ($=\partial \ln \omega_i/\partial P$), which are analogous to the Grüneisen parameter ($\gamma_i = B_0\,\partial(\ln \omega_i)/\partial P$). The Γ_i parameters for the materials investigated experimentally lie in the range (4.0–12.5) $\times$ 10^{-3} GPa^{-1} as can be seen in table 1. The fact that the Γ_i parameters lie in a relatively narrow region indicates that the binding forces are nearly of the same nature and order of magnitude. This is compatible with our theoretical results [13] that the majority of the Raman modes are not related solely to vibrations of certain molecular units of the $RE_3Al_5O_{12}$ compounds, but rather to a linear combination of them. Furthermore, the absence of Raman-active modes with frequencies below 100 cm^{-1} implies that strong interactions occur within various kinds of atom in these compounds. Usually in crystalline materials, containing a large number of atoms in their primitive cell, the lower-frequency modes, which are connected with translational motions of various subunits, have Grüneisen parameter values approximately an order of magnitude

larger than those for the higher-frequency ones [29]. However, in the $RE_3Al_5O_{12}$ compounds the lower-frequency modes ($\omega < 500$ cm^{-1}) have Γ_i values (see table 1) which are almost twice those of the higher-frequency ones. This experimental finding indicates that the binding forces between the molecular subunits in the $RE_3Al_5O_{12}$ modes have considerable strength. Thus, the pressure measurements show that the interpretation of the modes in the rare-earth aluminium garnets, in terms of internal and external modes, is a rough approximation and that the hierarchy of bonding interactions, in these compounds, is not well defined. This general picture concerning the strength of the interactions in the $RE_3Al_5O_{12}$ compounds combined with the high compactness of the garnet structure could, in some way, explain the absence of any phase transition in these materials in the pressure region investigated and as a matter of fact this phase stability extends well into the high-pressure region at least for the $Y_3Al_5O_{12}$ compound [21]. By assuming that the binding forces in the $RE_3Al_5O_{12}$ are of the same type, we can roughly estimate the corresponding Γ_k ($=(1/2)\,\partial(\ln k_i)/\partial P$) coefficient for the k-bond (tetrahedral, octahedral and dodecahedral). For $Yb_3Al_5O_{12}$ the Γ_k parameters lie in the range (5.1–9.8) $\times 10^{-3}$ GPa^{-1}, for $Tm_3Al_5O_{12}$ in the range (5.7–10.7) $\times 10^{-3}$ GPa^{-1}, while for $Dy_3Al_5O_{12}$ they lie in the range (5.5–20.0) $\times 10^{-3}$ GPa^{-1} indicating that only in $Dy_3Al_5O_{12}$ there is a clear differentiation of the bond stiffnesses. We mention that an analogous departure from the common behaviour is shown by $Dy_3Al_5O_{12}$, also for the effective charges and force constants under normal conditions (see table 2). This distinctive behaviour may be connected with the gradual increase of the occupation of the f electronic shells in the Dy ions.

5. Conclusions

In conclusion, we have investigated experimentally, by Raman spectroscopy at room temperature and theoretically by using a RIM, the effect of high hydrostatic pressure on various rare-earth aluminium garnet compounds. Under normal conditions we have resolved around 15 out of 25 expected Raman-active modes. The accidental degeneracy occurring in some modes is lifted upon application of high pressure due to the different pressure responses of the modes involved. On applying pressure, the overall profiles of the Raman modes do not change significantly; they exhibit a positive shift with pressure coefficients ranging between -0.1 and 5.6 cm^{-1} GPa^{-1}. On the basis of our theoretical analysis we have been able to clarify the symmetry assignment of the various Raman modes. Furthermore, we have shown that the interpretation of the observed Raman modes in $RE_3Al_5O_{12}$ compounds in terms of solely internal or external vibrations of certain subunits is a very crude approximation. This may be valid, to some degree, for the modes above 650 cm^{-1}. For a realistic description of the Raman modes in the $RE_3Al_5O_{12}$, a linear combination of the various vibrations of the various subunits is necessary. Finally, by combining the experimental and theoretical results we found that there is no clear hierarchy of the bonding interactions in these materials.

References

[1] Menzer G 1928 *Z. Kristallogr.* **69** 300
[2] Toncelli A, Tonelli M, Zannoni E, Cavalli E and Cialdi S 2001 *J. Lumin.* **92** 237
[3] Liu J and Vohra Y K 1994 *Appl. Phys. Lett.* **64** 3386
[4] Hömmerich U and Bray K L 1995 *Phys. Rev.* B **51** 8595
[5] *Landolt–Börnstein New Series* 1978 Group III, vol 12 (Berlin: Springer)
[6] Armbruster T, Geige C A and Lage G A 1992 *Am. Mineral.* **77** 515
[7] Harris J, Hutchison M T, Hursthouse M, Light M and Harte B 1997 *Nature* **387** 486
[8] Hurrell J P, Porto P S, Chang I F, Mitra S S and Bauman R P 1968 *Phys. Rev.* **173** 851
[9] Wandsack R L, Lewis J L, Argyle B E and Chang B K 1971 *Phys. Rev.* B **3** 4342

[10] Mace G, Schaack G, Ng Toaning and Koningstein J A 1969 *Z. Phys.* **117** 1308
[11] Song J, Kein J, Wadsack P B, Selders R L, Mroczkowski M and Chang S K 1973 *J. Opt. Soc. Am.* **63** 1135
[12] McDevitt N T 1969 *J. Opt. Soc. Am.* **59** 1240
[13] Papagelis K, Kanellis G, Kourouklis G A and Ves S *Phys. Status Solidi* b at press
[14] Xu Yong-Nian and Ching W Y 1999 *Phys. Rev.* B **59** 10 530
[15] Mittal R, Chaplot S L and Choudhury N 2001 *Phys. Rev.* B **4** 94 302
Mittal R, Chaplot S L, Choudhury N and Long C K 2000 *Phys. Rev.* B **1** 3983
[16] Jayaraman A 1986 *Rev. Sci. Instrum.* **57** 1013
[17] Jayaraman A 1983 *Rev. Mod. Phys.* **55** 6
[18] Barnett D, Block S and Piermarini G J 1973 *Rev. Sci. Instrum.* **44** 1
[19] Papagelis K, Kanellis G, Arvanitidis J, Kourouklis G A and Ves S 1999 *Phys. Status Solidi* b **215** 193
[20] Hua H, Liu J and Vohra Y K 1996 *J. Phys.: Condens. Matter* **8** 139
[21] Hua H, Mirov S and Vohra Y K 1996 *Phys. Rev.* B **54** 6200
[22] Bohr M and Huang K 1954 *Dynamical Theory of Crystal Lattices* (Oxford: Oxford University Press)
[23] Murnaghan F D 1944 *Proc. Natl Acad. Sci. USA* **30** 244
[24] Alton W J and Barlow A J 1967 *J. Appl. Phys.* **32** 1172
[25] Anderson O L 1966 *J. Phys. Chem. Solids.* **27** 547
[26] Trommer R, Müller H, Cardona M and Vogl P 1980 *Phys. Rev.* B **21** 4689
[27] Hazen R M, Down L W, Conrad P G, Finger L W and Gasparik T 1994 *Phys. Chem. Minerals* **21** 374
[28] Zhang L, Ahsbahs H, Kutoglu A and Geiger C A 1999 *Phys. Chem. Minerals* **27** 52
Zhang L, Ahsbahs H and Kutoglu A 1998 *Phys. Chem. Minerals* **25** 301 and references therein
[29] Weinstein B A and Zallen R 1984 *Light Scattering in Solids* vol 4, ed M Cardona and G Güntherodt (Heidelberg: Springer) and references therein